Contents

Chapter 5

Waves in the ocean

In this chapter we describe the general solution and dynamics of shallow-water waves and try to put them into a wider context, emphasizing their role in the ocean circulation and the coupled ocean-atmosphere system.

We will look for wave solutions of the shallow-water equations on the f-plane and β-plane. A few solutions will appear, some have already been discussed in different contexts, and some are new.

5.1 Poincaré Waves

We start by linearizing our shallow-water equations for a fluid $h = H + \eta$ over a state at rest

$$\boldsymbol{u} = u' \tag{5.1}$$
$$h = H + \eta \tag{5.2}$$

so that our equations, after eliminating higher order terms, reduce to

$$\frac{\partial u}{\partial t} - f_0 v = -g\frac{\partial \eta}{\partial x} \tag{5.3}$$
$$\frac{\partial v}{\partial t} + f_0 u = -g\frac{\partial \eta}{\partial y} \tag{5.4}$$
$$\frac{\partial \eta}{\partial t} + H\nabla \cdot \boldsymbol{u} = 0 \tag{5.5}$$

A dispersion relation can now be obtained by looking for wave solutions of the type

$$(u, v, \eta) = (u_0, v_0, \eta_0)e^{i(kx+ly-\omega t)} \tag{5.6}$$

into our linearized equations:

$$\begin{aligned} -u_0 i\omega - f_0 v_0 &= -g\eta_0 ik & (5.7)\\ -v_0 i\omega + f_0 u_0 &= -g\eta_0 il & (5.8)\\ -\eta_0 i\omega + H(iku_0 + v_0 il) &= 0 & (5.9) \end{aligned}$$

Non-trivial solutions of the system exist only if the determinant is equal to zero, so that

$$\begin{vmatrix} -i\omega & -f_0 & gik \\ f_0 & -i\omega & gil \\ ikH & ilH & i\omega \end{vmatrix} = 0 \tag{5.10}$$

and this is true if

$$\omega[\omega^2 - f_0^2 - gH(k^2 + l^2)] = 0 \tag{5.11}$$

Now, there are a few interesting possible solutions for the frequency ω.

The first case is

$$\boxed{\omega = 0} \tag{5.12}$$

This solution describes a time-independent flow and the equations describe a geostrophically balanced flow.

The second possible solution is if

$$\boxed{\omega^2 = f_0^2 + c^2(k^2 + l^2)} \tag{5.13}$$

where $c = (gH)^{1/2}$ is the gravity wave phase speed. The dispersion relation describes wave solutions of superinertial flow ($\omega > f_0$) which are called **Poincaré waves**. From this solution we can highlight three possible limiting cases (see Fig. 5.1).

First, the limit of no rotation, when $f_0 = 0$. The solution reduces to $\omega^2 = c^2K^2$ and the frequency solutions are

$$\boxed{\omega = \pm Kc} \tag{5.14}$$

where $K^2 = (k^2 + l^2)$, which describe a classical gravity wave.

Second, the short wave limit, when $K^2 \gg f_0^2/(gH)$, which gives

$$\boxed{\omega^2 = c^2K^2} \tag{5.15}$$

again, the dispersion relation is that of the non-rotating case with phase speed c. This is because

$$\frac{(2\pi)^2}{\lambda^2} \gg \frac{f^2}{gH} \quad \frac{2\pi}{\lambda} \gg \frac{f}{c} \quad \lambda \ll \frac{(gH)^{1/2}}{f} 2\pi \tag{5.16}$$

so that $L_d \gg \lambda$, where L_d is the Rossby radius $L_d = (gH)^{1/2}/f$. Basically, this solution looks like a gravity wave in a rotating case.

Third, the long wave limit, when $K^2 \ll f_0^2/(gH)$. In this case we have

$$\boxed{\omega^2 = f_0^2} \tag{5.17}$$

and therefore the Rossby radius is much smaller than the wave length, $L_d \ll \lambda$. In this limiting case, there is no space dependency, $k = l = 0$, and the surface elevation anomaly is also zero $\eta = 0$. The solution is

$$\frac{\partial u}{\partial t} - fv = 0 \tag{5.18}$$

$$\frac{\partial v}{\partial t} + fu = 0 \tag{5.19}$$

and these are called inertial oscillations, circulating at the planetary frequency $\omega = f$.

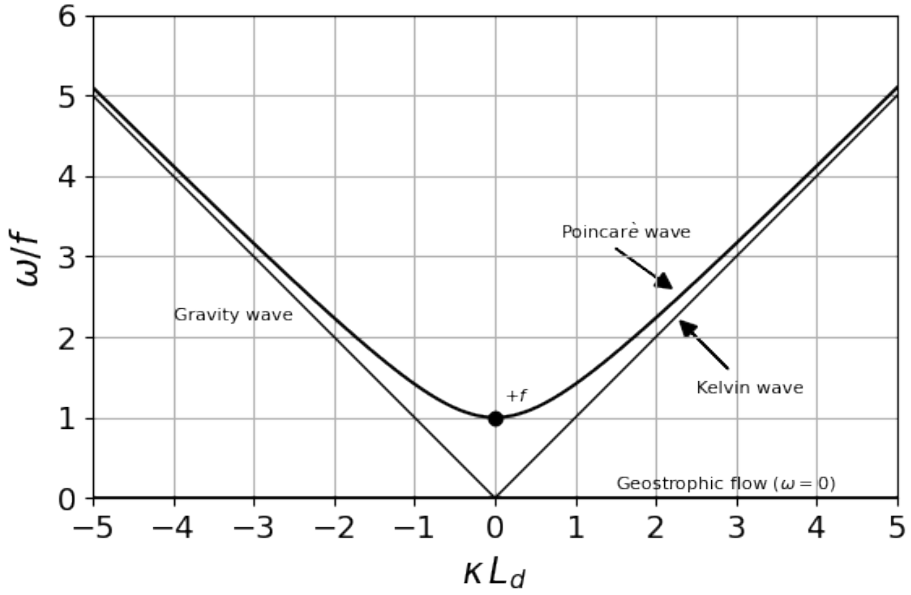

Figure 5.1: *Dispersion relation for Poincarè and Kelvin waves. The frequency is scaled by f and the wavenumber by L_d. The black dot marks the inertial oscillations regime and the $\omega = 0$ is the geostrophic case.*

5.2 Kelvin Waves

Kelvin waves are a particular solution of the shallow water equations describing a gravity wave that exists in a rotating frame and with the help of lateral boundaries. We could show Kelvin waves propagating in a channel, with two parallel boundaries, but for a start we will consider the case of a single lateral boundary. The first assumption is that, if $u = 0$ at the boundary, we could simply consider the zonal component of the velocity zero everywhere. The meridional component is not zero at the boundary, because the flow is frictionless. The linearized shallow water equations are

$$-f_0 v = -g\frac{\partial \eta}{\partial x} \tag{5.20}$$

$$\frac{\partial v}{\partial t} = -g\frac{\partial \eta}{\partial y} \tag{5.21}$$

$$\frac{\partial \eta}{\partial t} + H\frac{\partial v}{\partial y} = 0 \tag{5.22}$$

Continuity becomes, after differentiating with respect to y

$$\frac{\partial \eta}{\partial t \partial y} = -H\frac{\partial^2 v}{\partial y^2} \tag{5.23}$$

and using the momentum equation

$$\frac{\partial^2 v}{\partial t^2} = gH\frac{\partial^2 v}{\partial y^2} \tag{5.24}$$

which is the standard wave equation with phase speed $c = (gH)^{1/2}$. The solution to this is

$$v = V_1 \cos k(y - ct) + V_2 \cos k(y + ct) \tag{5.25}$$

and the wave propagates along the meridional boundary. Substituting this solution into the momentum equation we obtain a solution for η

$$\eta = V_1 \frac{c}{g} \cos k(y - ct) - V_2 \frac{c}{g} \cos k(y + ct) \tag{5.26}$$

which describes a propagating wave in terms of surface elevation. The solution has been found for both v and η with no Coriolis term: this has the characteristics of a non-rotating shallow water wave. The velocity is

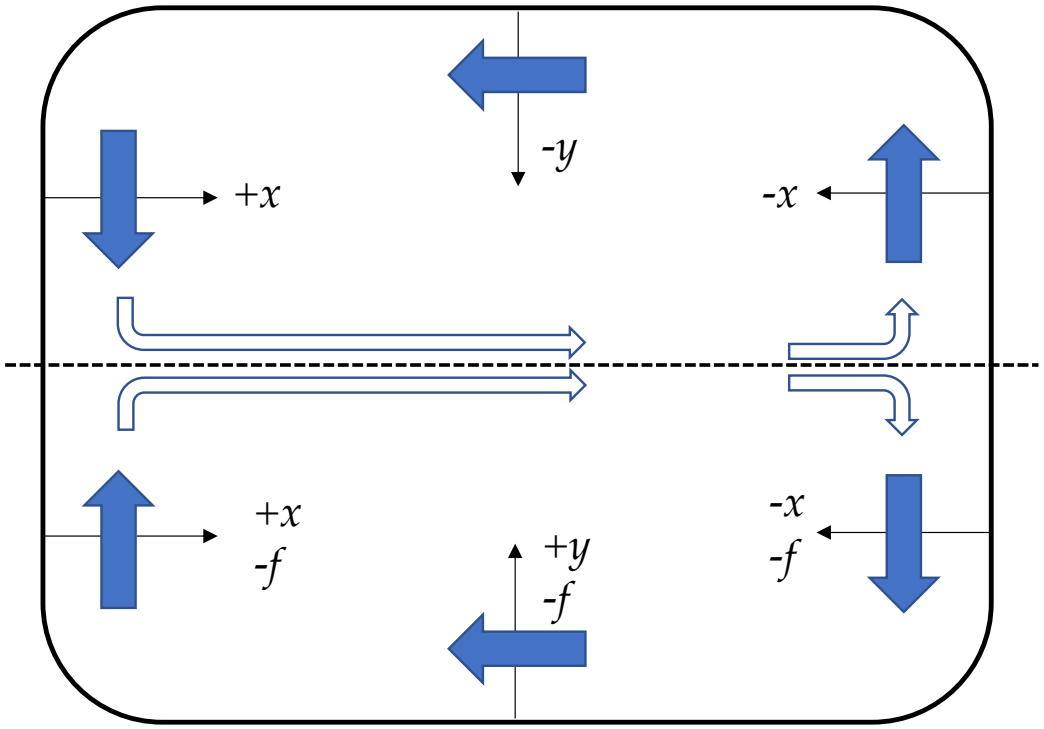

Figure 5.2: *For a system bounded to the west (x positive) the wave propagates in the negative y direction, i.e. to the south. If x is negative this reverses so on the eastern side of the basin the Kelvin wave propagates northwards. In the northern hemisphere a Kelvin wave will keep the coast to its right as it pushed against it by the Coriolis force.*

in geostrophic balance with the pressure field, although it is a wave and $\omega \sim f$.

The solutions in the x-direction are

$$V_1 = e^{(f_0/c)x} \tag{5.27}$$

$$V_2 = e^{-(f_0/c)x} \tag{5.28}$$

and remember that $f_0/c = L_d^{-1}$. The first solution grows exponentially for positive x away from the meridional boundary, which is not physically possible. We are then left with the following set of solutions

$$v = e^{-x/L_d} \cos k(y + ct) \tag{5.29}$$

$$u = 0 \tag{5.30}$$

$$\eta = -e^{-x/L_d} \frac{c}{g} \cos k(y + ct) \tag{5.31}$$

$$= -(H/g)^{1/2} e^{-x/L_d} \cos k(y + ct) \tag{5.32}$$

These are Kelvin waves. They are trapped by the meridional boundary and decay exponentially away from it. The trapping spatial scale is given by the Rossby radius, and for f_0 positive the boundary is at the right of the wave propagation. Kelvin waves are balancing f against the wall, which could be a topographic boundary or a waveguide such as the equator (Fig. 5.2).

Barotropic Kelvin waves are also tidal waves, propagating around an amphidromic point .

5.3 Planetary, or Rossby, waves

The time-dependent ocean circulation has an important impact on our climate due to the ocean large heat capacity. Any abrupt change, the intrinsic variability and possible variations of the general circulation caused by the atmospheric influence is fundamental in climate studies. Moreover, the oceans are no longer considered passive in the atmosphere-ocean system, but contribute to the production of the climate low-frequency variability at interannual to decadal time scales (*Talley*, 1999; *Dewar*, 2001; *Pierce et al.*, 2001).

The discovery of Planetary waves by the solution of Laplace's equation as the second class waves dates back to the late nineteenth century by *Hough* (1897). Later C.G. Rossby pointed out the characteristic of these waves, hence they carry his name and are also called Rossby waves.

Since then, Rossby wave theory is well known (*Gill*, 1982; *Dickinson*, 1978; *Leblond and Mysak*, 1981) and is usually applied to an ocean at rest with uniform depth. Rossby waves owe their existence to the meridional variation of the Coriolis force (the β effect) and therefore propagate following an east-west waveguide, as the conservation of potential vorticity is their restoring force. These kinds of waves, whose frequencies are considerably lower than those of gravity waves and are subinertial ($\omega \ll f$), are also sometimes called quasigeostrophic waves, with a dynamic evolution depending on the departure from geostrophy.

The generation of these waves is still not completely understood but the main forcing is wind stress and buoyancy forcing, though the latter is thought to act in a minor way, and upwelling-downwelling on the eastern boundary (*Leblond and Mysak*, 1981; *Gill*, 1982).

The oceans are forced at the surface by the wind frictional stress and Rossby waves appear to play a fundamental role in redistributing and dispersing large-scale time-varying energy in the ocean. The propagation of Rossby waves towards the ocean interior under the influence of wind stress results in establishing a Sverdrup balance in the basin, accumulating energy in the western boundaries and intensifying currents there (*Anderson and Gill*, 1975, 1979).

Due to the ubiquitous presence of Rossby waves in the world oceans they influence ocean gyres and air-sea fluxes at all latitudes, affecting in turn the atmospheric heat transport and circulation. They are believed to provide teleconnections between the equatorial and middle latitudes regions (*Galanti and Tziperman*, 2003) as well as transhemispheric and interbasin communications (*Cessi and Otheguy*, 2003). Other major effects are the maintenance and intensification of western boundary currents, trans-

port of a large amount of heat and, because of their time-scale, they play a key role in the climate system.

Rossby waves are very long waves so that the f-plane is not a good approximation anymore and we will build our solutions on the β-plane. The frequency is going to be subinertial, $\omega \ll f$, and so they are close to geostrophy.

Our set of equations is

$$\frac{\partial u}{\partial t} - (f_0 + \beta y)\, v = -g\frac{\partial \eta}{\partial x} \tag{5.33}$$

$$\frac{\partial v}{\partial t} + (f_0 + \beta y)\, u = -g\frac{\partial \eta}{\partial y} \tag{5.34}$$

$$\frac{\partial \eta}{\partial t} + H\left(\frac{\partial u}{\partial x} + \frac{\partial v}{\partial y}\right) = 0 \tag{5.35}$$

Given that $\omega \ll f$, $\frac{\partial}{\partial t} \ll 1$ and $\beta L/f_0 \ll 1$ we can approximate the momentum equations to a geostrophic flow

$$-f_0 v = -g\frac{\partial \eta}{\partial x} \tag{5.36}$$

$$f_0 u = -g\frac{\partial \eta}{\partial y} \tag{5.37}$$

and adding these geostrophic solutions to the shallow water equations

$$-f_0 v = -g\frac{\partial \eta}{\partial x} + \beta y \frac{g}{f_0}\frac{\partial \eta}{\partial x} + \frac{g}{f_0}\frac{\partial^2 \eta}{\partial y \partial t} \tag{5.38}$$

$$f_0 u = -g\frac{\partial \eta}{\partial y} + \beta y \frac{g}{f_0}\frac{\partial \eta}{\partial y} - \frac{g}{f_0}\frac{\partial^2 \eta}{\partial x \partial t} \tag{5.39}$$

The first part of the momentum equations is that of a geostrophic flow and the remaining is the small contribution from variations induced by the **ageostrophic component**. The last terms will be responsible for the propagation of Rossby waves.

Using continuity and (5.38)-(5.39) we arrive to

$$\frac{\partial \eta}{\partial t} - L_d^2 \partial_t \nabla^2 \eta - \beta L_d^2 \frac{\partial \eta}{\partial x} = 0 \tag{5.40}$$

which is a leading order approximation to the potential vorticity equation describing a quasi-geostrophic flow

$$\partial_t \left(\nabla^2 \eta - L_d^{-2} \eta\right) + \beta \frac{\partial \eta}{\partial x} = 0 \tag{5.41}$$

Now we can look for Fourier type solutions in the form $\eta = \eta_0 e^{i(kx+ly-\omega t)}$

$$\boxed{\omega = -\frac{\beta k}{(k^2+l^2)+L_d^{-2}}} \tag{5.42}$$

or alternatively

$$\omega = -\beta L_d^2 \frac{k}{1+L_d^2(k^2+l^2)} \tag{5.43}$$

Evidently, on the f-plane ($\beta = 0$) the solution reduces to a geostrophic flow and no wave is allowed to propagate. **The meridional gradient in f is thus the restoring force for Rossby waves**.

Two possible cases can be envisaged, setting $l = 0$.

First, that of short waves, where $L \leq L_d$ and therefore $kL_d \geq 1$, for L a typical scale of the wave length and k a typical scale of the wave number. In this case the dispersion relation reduces to

$$\omega = -\beta L_d^2 \frac{k}{L_d^2(k^2)} = -\frac{\beta}{k} = -\beta L \tag{5.44}$$

Given that we are on the β-plane approximation, $\beta y \ll f_0 \rightarrow \beta L \ll f_0 \rightarrow \omega \ll f_0$, confirming the subinterial period.

Second, waves could have very long wave length $L \geq L_d$ or $kL_d \leq 1$

$$\omega = -\beta L_d^2 k = -\beta \frac{L_d^2 k^2}{k} \ll -\frac{\beta}{k} = -\beta L \tag{5.45}$$

and therefore $\omega \ll f_0$. The period of Rossby waves is always subinertial.

5.3.1 Phase and group speeds

Keeping $l = 0$ and using the following scaling

$$\omega = \hat{\omega}\beta L_d \tag{5.46}$$

$$\kappa = \frac{\hat{\kappa}}{L_d} \tag{5.47}$$

The dispersion relation takes the form

$$\hat{\omega}\beta L_d = -\beta L_d^2 \frac{\hat{\kappa}/L_d}{1+L_d^2\frac{\hat{\kappa}^2}{L_d^2}} \tag{5.48}$$

$$\hat{\omega} = -L_d \frac{\hat{\kappa}/L_d}{1+\hat{\kappa}^2} = -\frac{\hat{\kappa}}{1+\hat{\kappa}^2} \tag{5.49}$$

and for $|\hat{\kappa}| = -1$ the frequency takes the value $|\hat{\omega}| = -0.5$ (see Fig. 5.3).

The phase speed of Rossby waves is easily computed (with $l = 0$), using (5.42)

$$\boxed{c_p = \frac{\omega}{k} = \frac{-\beta}{k^2 + L_d^{-2}}} \tag{5.50}$$

it is always negative and larger for long waves.

For long Rossby waves, the phase velocity is approximated by

$$\boldsymbol{c_p} = \omega/\kappa = -\beta L_d^2 \tag{5.51}$$

which is strictly westward even if $l \neq 0$.

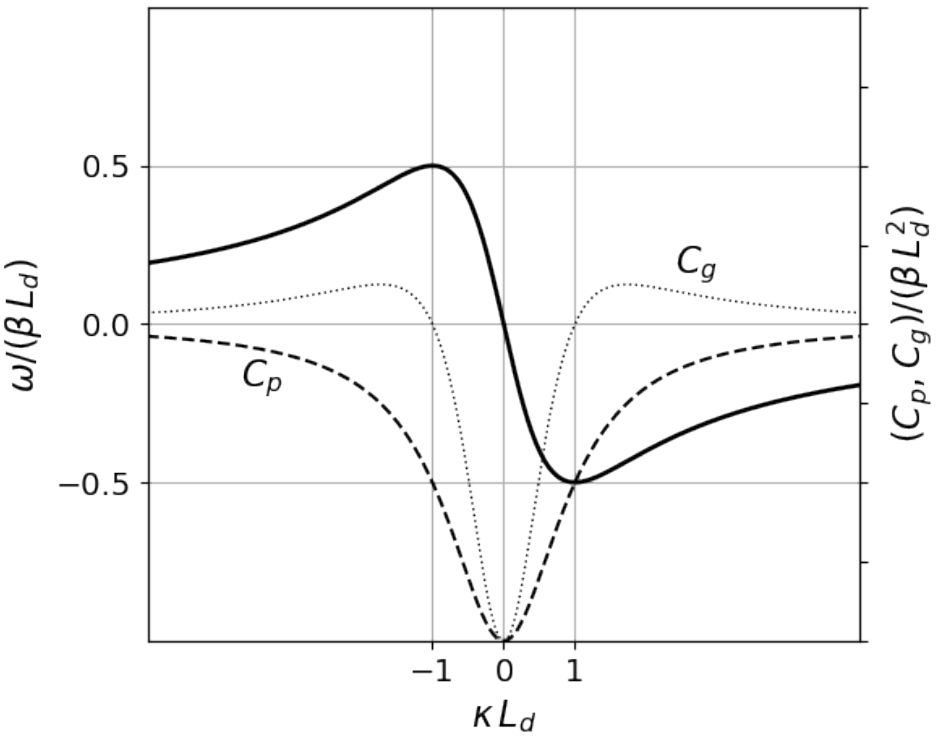

Figure 5.3: *Rossby wave dispersion relation, phase and group speeds. Phase velocities, C_p, are always westward. Group velocities, C_g, are westward for long waves ($\kappa < -1$) and eastward for short waves ($\kappa > -1$). The cutoff frequency is set at $\beta L_d/2$.*

The phase speed is always negative but is the energy flux always directed westward? this does not seem possible.

The group velocity is obtained by differentiating the dispersion relation

$$\boldsymbol{c_g} = (\frac{\partial \omega}{\partial \kappa}, \frac{\partial \omega}{\partial l}) = \beta(\kappa^2 - l^2 - L_d^{-2}, 2\kappa l)/(\kappa^2 + l^2 + L_d^{-2})^2 \tag{5.52}$$

or, by setting $l = 0$

$$\boldsymbol{c_g} = \frac{\beta\kappa^2 - \beta L_d^{-2}}{(\kappa^2 + L_d^{-2})^2} \tag{5.53}$$

By setting $k = 0$, group and phase velocities are now equal $c_p = c_g = -\beta L_d^2$ (see Fig. 5.3), and long waves are therefore non-dispersive.

If $l \neq 0$ the dispersion relation takes the form of the dispersion diagram in Fig. 5.4. The group velocity, the gradient of the frequency in wavenumber space, is normal to the contours and inversely proportional to the spacing between contours. The hyperbola separating waves with eastward and westward group velocity is shown by the dashed line and is $\kappa^2 = l^2 + L_d^{-2}$. Frequency contours reduce to a single point when $\omega = 0.5\beta L_d$ and $\kappa = L_d$.

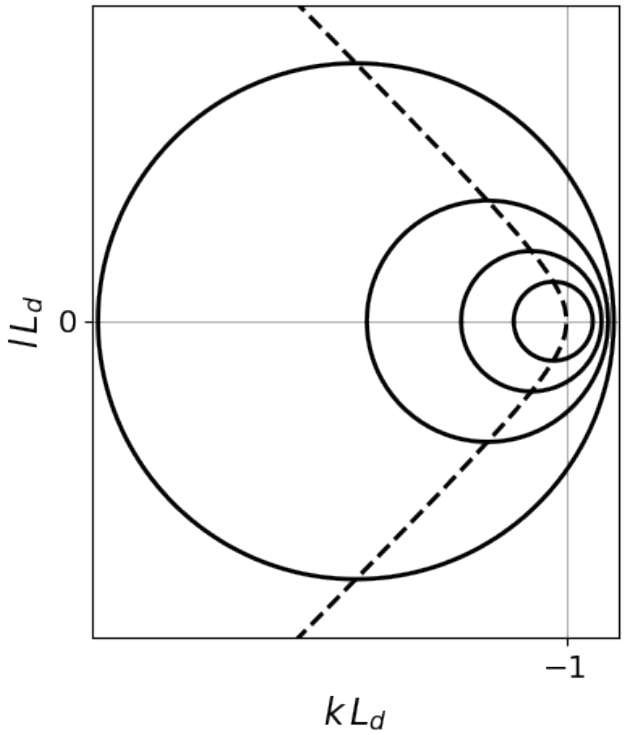

Figure 5.4: *Rossby wave dispersion diagram. Contours are of frequency in units of $\beta\, L_d$. The group velocity, the gradient of the frequency in wavenumber space, is normal to the contours and inversely proportional to the spacing between contours. The hyperbola separating waves with eastward and westward group velocity is shown by the dashed line and is $\kappa^2 = l^2 + L_d^{-2}$. Frequency contours reduce to a single point when $\omega = 0.5\beta L_d$ and $\kappa = L_d$.*

5.3.2 Quasi-geostrophic Rossby waves

In order to obtain and describe the Rossby wave solutions, we consider the linearised quasi-geostrophic (QG) potential vorticity equation (*Pedlosky*, 1987):

$$\partial_t q_i + J(\psi_i, q_i) = 0, \tag{5.54}$$

where $J(a,b) = a_x b_y - a_y b_x$ is the Jacobian and ψ the stream function. Introducing a plane wave solution of the type $\psi = \Psi e^{i(kx+ly-\sigma t)}$ into (5.54) we naturally obtain the dispersion relation for Rossby waves, showing their basic characteristics (*Leblond and Mysak*, 1981; *Gill*, 1982)

$$\omega = -\frac{\beta k}{(k^2+l^2)+L_d^{-2}},$$

where ω is the frequency, k and l are the horizontal wavenumber, β is the meridional variation of the Coriolis parameter and L_d the Rossby radius (C^2/f^2). It is clear that Rossby waves have westward phase velocities (of the order of a few cm/s) and that these are increasing toward the equator (where equatorial wave theory holds) with a maximum speed $C_p = \beta L_d^2$. Group velocities, C_g, in the case of long waves, are westward and the waves are nondispersive ($C_g = C_p$), while short waves propagate eastwards but with very slow speeds.

Another remarkable feature of the planetary wave dispersion relation is that not all frequencies exist, with a cutoff frequency at $\frac{1}{2}\beta L_d$.

Besides the horizontal problem, the vertical one is of great importance. Using a normal mode representation (*Leblond and Mysak*, 1981), separating the vertical and horizontal structure, we find an infinite set of solutions (or normal modes). The zeroth is the barotropic one, almost vertically independent and very rapid; the other solutions, or modes, are called baroclinic with decreasing phase speeds and increasing oscillation in the vertical. A first-mode baroclinic Rossby wave takes months to years to cross an ocean basin, depending on the latitude.

A 3-layer model

In the case of a 3-layer ocean, the potential vorticities are given by

$$\begin{aligned} q_1 &= \nabla\psi_1 + \beta y - F_{11}(\psi_1 - \psi_2) \\ q_2 &= \nabla\psi_2 + \beta y - F_{21}(\psi_2 - \psi_1) - F_{22}(\psi_2 - \psi_3) \\ q_3 &= \nabla\psi_3 + \beta y - F_{32}(\psi_3 - \psi_2), \end{aligned}$$

where $F_{m,n} = f_0^2/(H_m g'_n)$ and g'_i and H_i are the reduced gravities and layer depths respectively.

For this 3-layer system, substitution of a plane wave solution leads to a generalised eigenvalue problem of the form $\mathsf{A}\Psi = \omega \mathsf{B}\Psi$, or explicitly:

$$\begin{bmatrix} \beta_1 & 0 & 0 \\ 0 & \beta_2 & 0 \\ 0 & 0 & \beta_3 \end{bmatrix} \begin{bmatrix} \psi_1 \\ \psi_2 \\ \psi_3 \end{bmatrix} = \omega \begin{bmatrix} -G_1 & 1 & 0 \\ G_2 & -G_3 & 1 \\ 0 & 1 & -G_4 \end{bmatrix} \begin{bmatrix} \psi_1 \\ \psi_2 \\ \psi_3 \end{bmatrix},$$

where $\beta_1 = (k\beta)/F_{11}$, $\beta_2 = (k\beta)/F_{22}$, $\beta_3 = (k\beta)/F_{32}$ and $G_1 = (K^2 + F_{11})/F_{11}$, $G_2 = F_{21}/F_{22}$, $G_3 = (K^2 + F_{21} + F_{22})/F_{22}$, $G_4 = (K^2 + F_{32})/F_{32}$, where $K^2 = k^2 + l^2$.

The solution of the system is plotted in Fig.5.5 and it describes the basic properties of Rossby wave propagation. In fact, for the 3-layer system, the dispersion relation is found on the upper panel and both phase and group velocities on the bottom panel of Fig.5.5. We can distinguish the barotropic mode with increasing frequencies towards long wavelengths, very fast phase speeds and positive (eastward) group velocities. The baroclinc modes have smaller frequencies, their phase velocities are always westward but their group velocities turn from westward to eastward at the point of maximum frequency

$$kL_d = |1| \text{ and } \omega(\beta L_d)^{-1} = |0.5| \tag{5.55}$$

where the group velocity is zero. Therefore, long baroclinic waves direct their energy westward while short waves direct it eastward. This means that, in the limit of long wavelengths, the phase and group speeds are the same and the waves are nondispersive. On the other hand, for short waves phase and group speeds differ and the waves are dispersive. The maximum group and phase velocity ($C_p = C_g = -\beta L_d^2$) are attained for long waves, they are to the west and can be found on the axis origin of the dispersion relation.

The system could be extended to an N-layer or even to a continuously stratified ocean. In every case, the solutions obtained are one barotropic and N-1 baroclinic modes of decreasing phase speeds. This method of analysis is called the *normal modes method*, in which the ocean is decomposed into an infinite set of solutions (or modes): one barotropic (or external) and the remaining baroclinic (or internal).

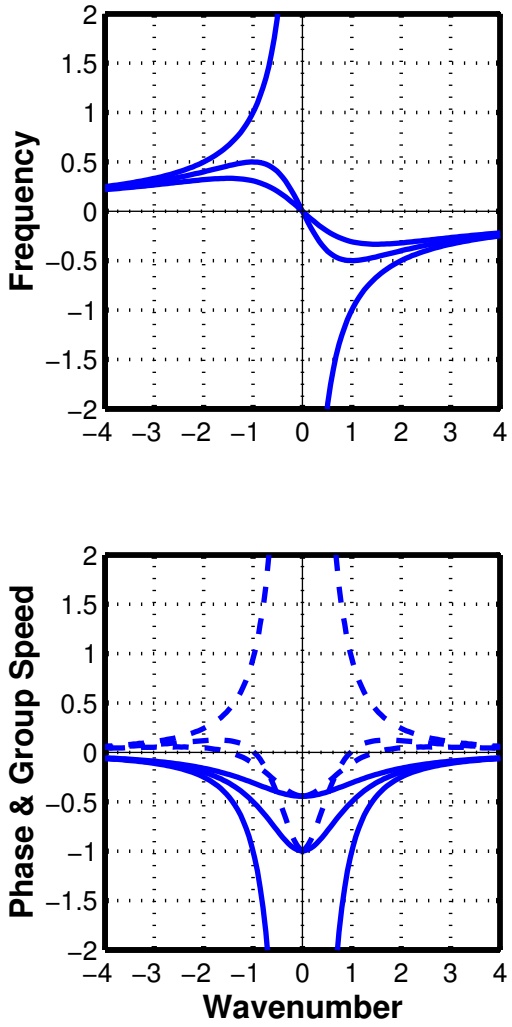

Figure 5.5: Upper panel: the dispersion relation for the barotropic and first two baroclinic modes of the 3-layer QG ocean. Shown are values of both positive and negative wavenumbers. The wavenumber is scaled by the deformation radius L_d and the frequency by βL_d; the meridional wavenumber l is set to zero. The first baroclinic mode frequency reaches a maximum at $\omega_{max} = \beta L_d/2$, i.e. $\omega_{max} = |0.5|$. Lower panel: phase (solid lines, $C_p = \omega/k$) and group (dashed lines, $C_g = \partial\omega/\partial k$) velocities of the barotropic and first two baroclinic modes, scaled by βL_d^2.

5.3.3 Rossby waves in observations and models

Chelton and Schlax (1996) presented for the first time the results of these observations identifying clear Rossby waves signals (Fig.5.6) and common features like the increase of phase speed in the western basin, the effect of bottom topography, eastward propagating equatorially trapped Kelvin waves and pulses related to El Niño events.

As anticipated, the advent of satellite altimetry brought a powerful tool to describe Rossby waves in the real ocean. The TOPEX/POSEIDON (T/P) altimeter is able to detect long baroclinic planetary waves unambiguously over the entire world ocean (Fig. 5.7).

The T/P altimetry data reveal the sea surface height anomalies (SSHA) and to analyse this data time-longitude plots, known as Hovmöller diagrams, are used, which clearly show Rossby waves as diagonal alignments of crests and troughs moving westward. An example of this is given in Fig.5.7, where SSHA data from the Indian Ocean are plotted for the latitude 20^oS from 1993 till May 2005; in the left panel the row data are plotted while in the right panel the data have been filtered with a westward filter to better show Rossby wave propagation.

By this technique, Rossby waves are detected in all basins and altimetry has been used also in the Southern Ocean (*Hughes*, 1995) where two dynamical systems were found, a supercritical and a subcritical one with respect to Rossby waves, the first one being able to advect the waves east-

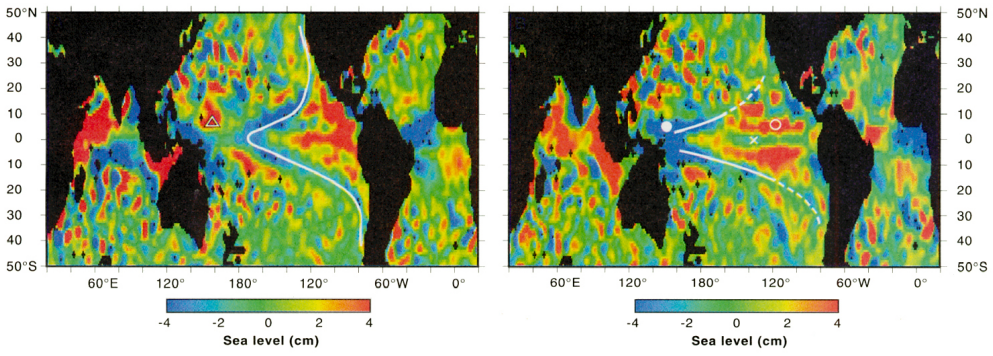

Fig. 4. Global maps of filtered sea level (*22*) on (**A**) 13 April 1993 (cycle 21) and 3.5 months later on (**B**) 31 July 1993 (cycle 32). White lines identify a westward-propagating, β-refracted Rossby wave trough. The time evolutions of the equatorial Kelvin wave trough (X), the Rossby wave crests (open triangle and open circle), and the Rossby wave trough (solid circle) can be traced from the times and locations of the matching symbols in Fig. 3. These two maps are frames from an animation of TOPEX/POSEIDON data that is available on the World Wide Web at http://topex-www.jpl.nasa.gov/contrib/chelton/rossby/.

Figure 5.6: Sea surface height anomalies showing the propagation of planetary waves in the Pacific Ocean. Also clear is the β-effect inducing larger phase speeds towards the equator [from *Chelton and Schlax* (1996)].

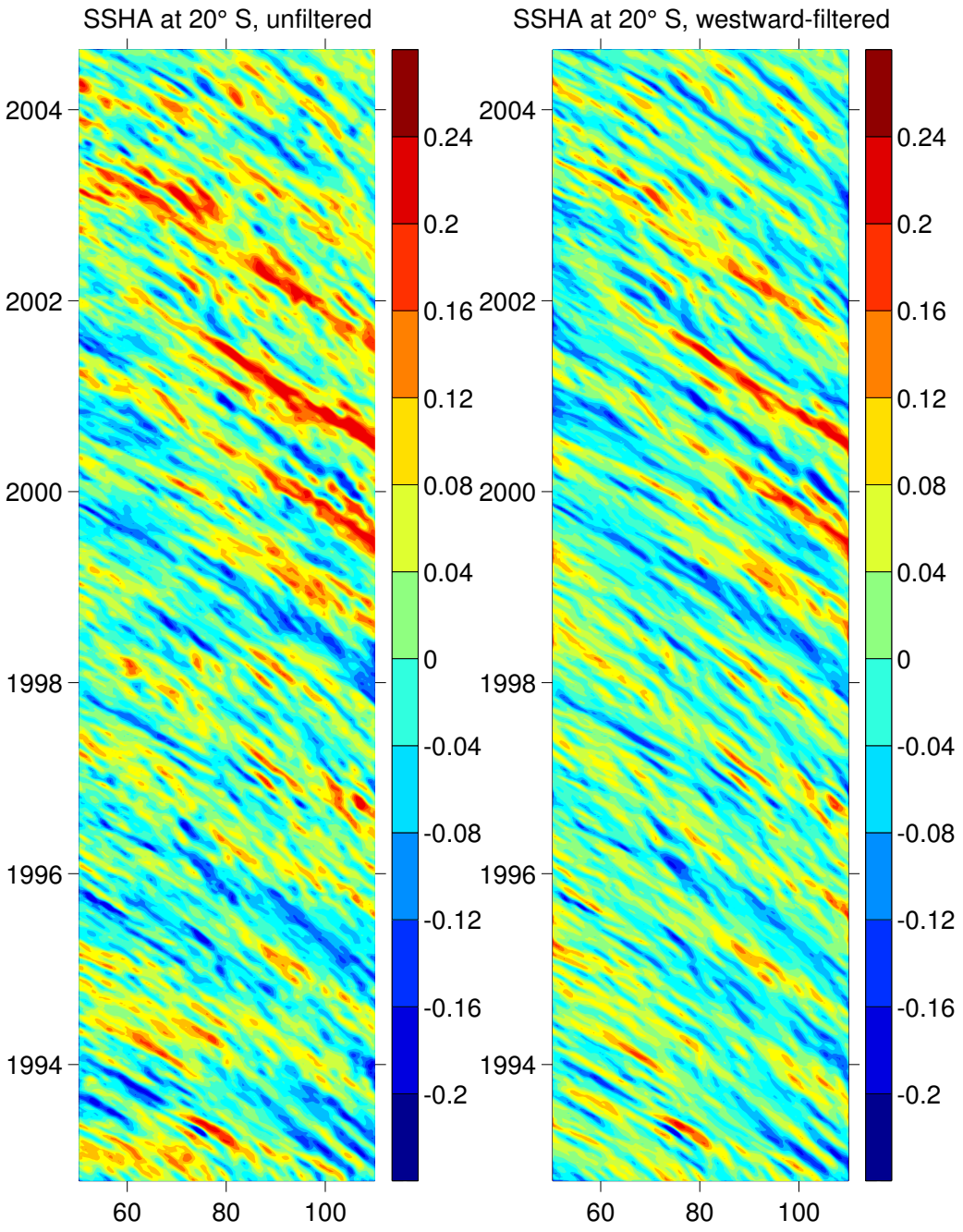

Figure 5.7: Time-longitude plot of the sea surface height anomalies (in meters) in the Indian Ocean at 20^oS. On the left panels, the original altimeter data. On the right panel, the corresponding westward-filtered signature. There is a clear evidence of crests and troughs propagating westward with a biannual period (Courtesy of P. Cipollini).

ward.

Rossby waves are also detected by other sensors like the Along-track Scanning Radiometer (ATSR) in sea surface temperature (SST) and, recently, SeaWiFS in ocean colour.

As an example, *Hill et al.* (2000) used a SST record to compute Rossby wave phase speeds finding good agreement with *Killworth et al.* (1997). They were also able to detect topographic effects such as those predicted by *Killworth and Blundell* (1999).

One of the latest applications has been using ocean colour. *Cipollini et al.* (2001) found for the first time Rossby waves in SeaWiFS datasets, although they are neither very clear nor ubiquitous. A preliminary explanation for this detectability was in term of the vertical displacements of the thermocline associated with the Rossby wave and subsequently changes in the nutrient upwelling.

5.3.4 Computing Rossby wave phase speeds

In order to compute the gravity wave phase speeds and Rossby radii of deformation we need to solve the generalized eigenvalue problem of Sturm-Liouville form:

$$\frac{d^2\phi}{dz^2} + \frac{N^2(z)}{C^2}\phi = 0 \tag{5.56}$$

subject to the following boundary conditions

$$\phi = 0 \qquad at \quad z = 0, -H \tag{5.57}$$

where H is the local mean water depth and N^2 is the Brunt-Väisälä frequency, computed from the potential density method as outlined in *Chelton et al.* (1998). Solution of the system (5.56)-(5.57) leads to an infinite set of eigenvalues C_m^{-2}, the baroclinic gravity wave phase speeds, and corresponding eigenfunctions ϕ_m.

However, *Chelton et al.* (1998) showed that a WKB approximation of the gravity wave speed is generally in good agreement with the solution given by the system (5.56)-(5.57), and this is:

$$C_m \approx C_m^{WKB} = (m\pi)^{-1} \int_{-H}^{0} N(z)\mathrm{d}z, \quad m \geq 1. \tag{5.58}$$

Then, within the extratropical regions, the Rossby radii of deformation are simply found by applying

$$L_d^m = \frac{C_m}{|f(\theta)|}. \tag{5.59}$$

We will be focusing on extratropical regions only ($|\theta| \geq 10^\circ$), leaving the equatorial wave dynamics response aside.

Now, we can compute the unperturbed long Rossby wave speeds

$$c_m = -\beta C_m^2 / f^2. \tag{5.60}$$

Since model data provide potential density ρ_θ, we can compute the stratification directly from the potential density method of the non-equispaced vertical levels k:

$$N^2(z) = -g/\rho_0 \Big[\rho_\theta(z) - \rho_\theta(z+1)/(\delta k(z) - \delta k(z+1))\Big] \tag{5.61}$$

The gravity wave speed can be obtained from two different method. First, as a good approximation, we can infer it from the WKB method as suggested in *Chelton et al.* (1998):

$$C_m = (m\pi)^{-1} \int_{-H}^{0} N(z)\mathrm{d}z, \quad m \geq 1. \tag{5.62}$$

After obtaining N^2 and C_m, the Rossby radii of deformation are readily computed as

$$L_d^m = \frac{C_m}{|f(\theta)|}, \quad |\theta| \geq 5^\circ \tag{5.63}$$

$$L_d^m = \frac{C_m}{2|\beta(\theta)|}, \quad |\theta| \leq 5^\circ. \tag{5.64}$$

or, for the extratropical band: $L_d^m = (|f|m\pi)^{-1} \int_{-H}^{0} N(z)\mathrm{d}z$

For the linear, long and extratropical waves, we can simply compute the Rossby wave phase speed as

$$c_m = -\beta (L_d^m)^2 \tag{5.65}$$

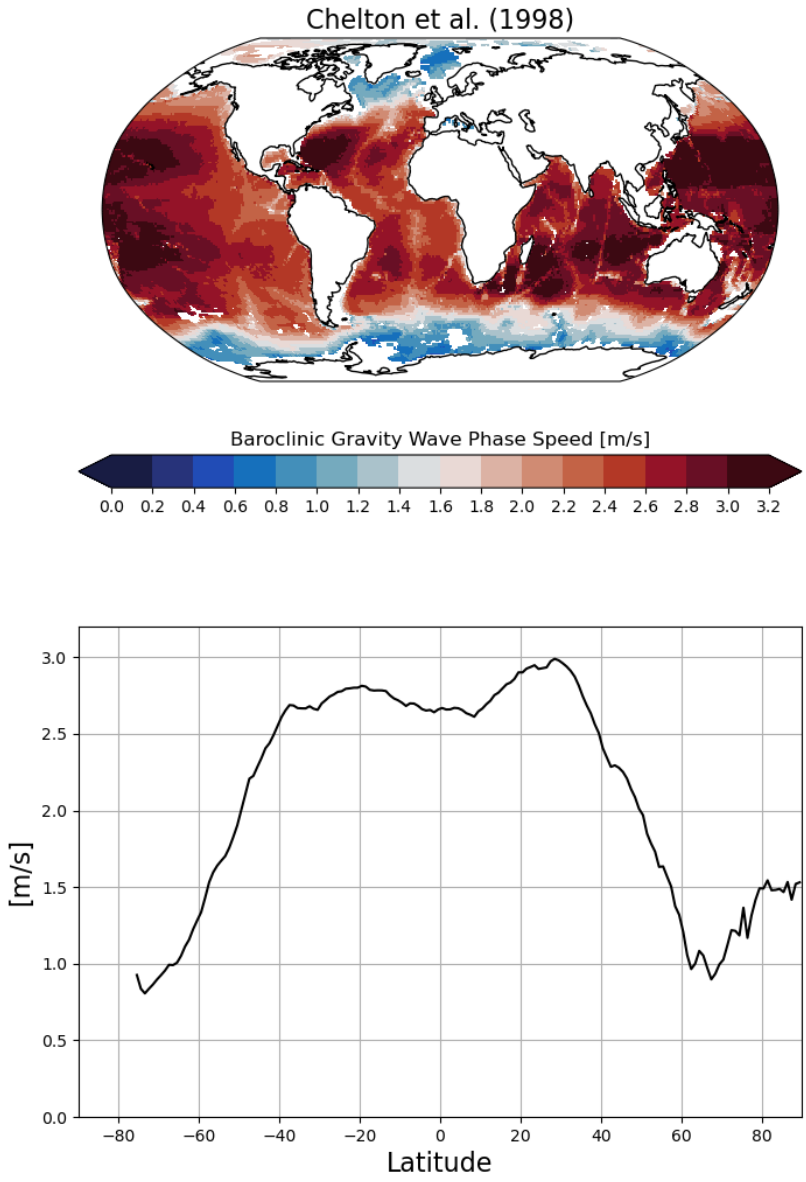

Figure 5.8: *A global contour map of the baroclinic gravity wave phase speed [from Chelton et al., 1998] and its zonal mean.*

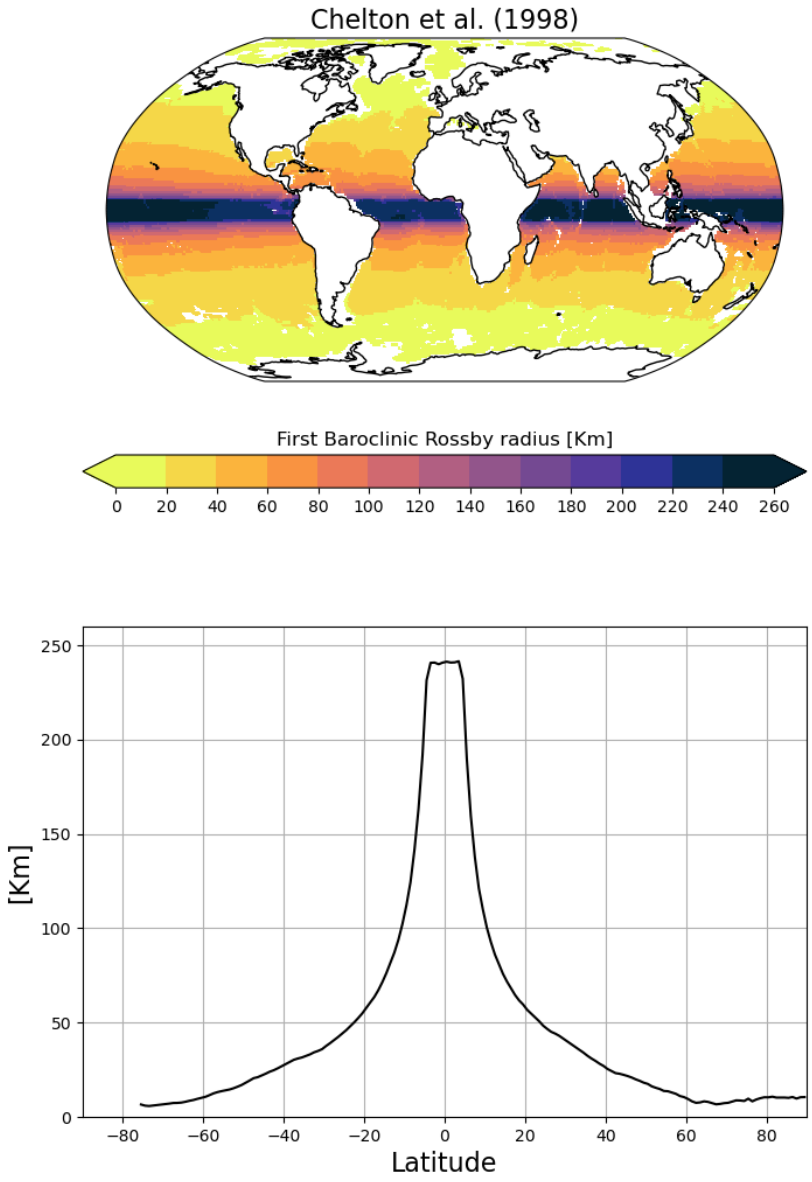

Figure 5.9: *A global contour map of the baroclinic Rossby radius of deformation and its zonal mean. [data from Chelton et al., 1998]*

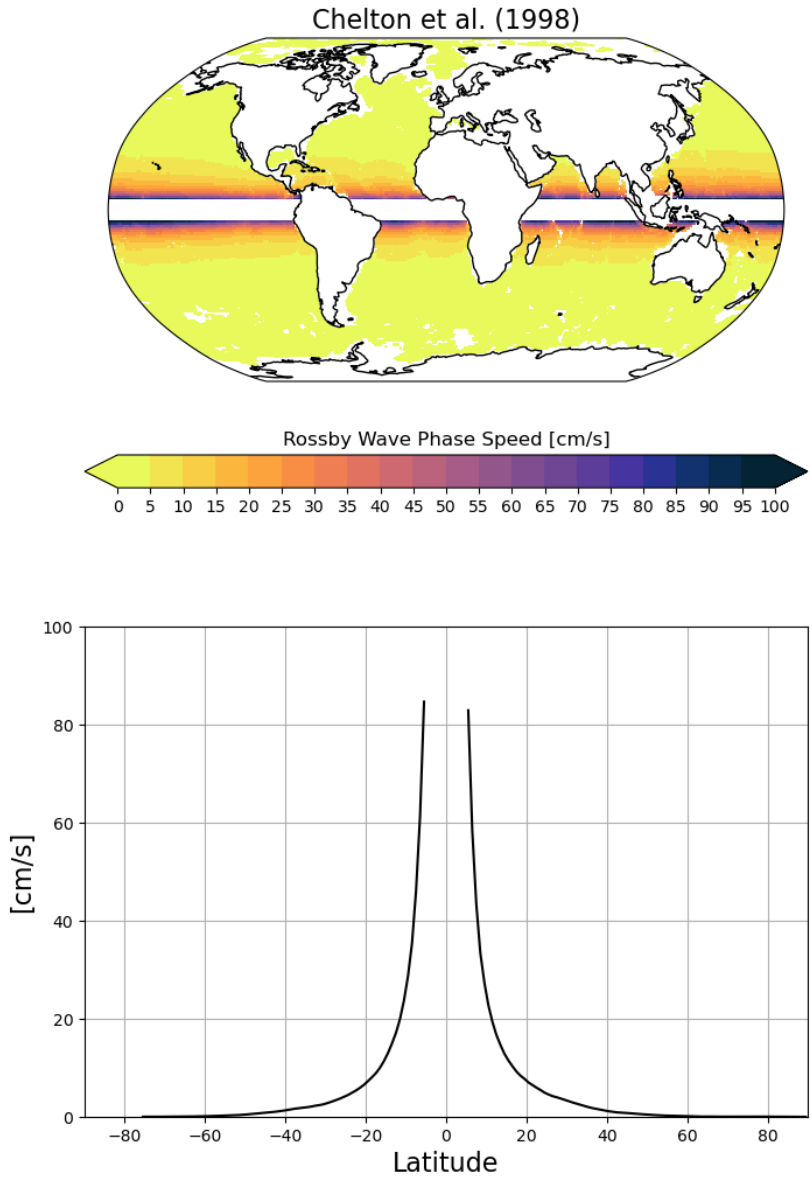

Figure 5.10: *A global contour map of the baroclinic Rossby wave phase speed and its zonal mean. [data from Chelton et al., 1998]*

5.4 Kelvin and Rossby waves in the general oceanic adjustment

The importance of Rossby waves in the spinup of the ocean and in the adjustment of the ocean interior was also recently shown by *Johnson and Marshall* (2002). They proposed a theory for surface Atlantic response to thermohaline variability; in their work they study the reaction of the ocean to a perturbation of the rate of deep water formation at high latitudes. These changes initiate Kelvin waves which propagate along the western boundary, in a similar response of that demonstrated by *Kawase* (1987), and then cross the basin as equatorial Kelvin waves until they reach the eastern boundary where they propagate northwards and southwards. The final part of the response is the radiation of Rossby waves from the eastern boundary, communicating the thermocline displacement to the ocean interior which is clearly illustrated with a series of snapshots (Fig. 5.11).

5.4.1 Implications in climate change scenarios

Saenko (2006) recently showed that, within the IPCC models, there is clear evidence of an increase of the first baroclinic Rossby radius with increasing oceanic stratification in the warmer climate. The changes range from 15 to 20% depending on the model and latitude. This would imply a greater length scale for mesoscale eddies and modified characteristics for oceanic Rossby waves, whose speed is proportional to the squared baroclinic Rossby radius of deformation. Also, the adjustment time scale in the ocean would decrease as well as in any ocean-atmosphere climate variability process where Rossby waves set the dominant period. Equally important, if not more in certain basins, is the change in the background baroclinic mean flow and its subsequent effect on the propagation of Rossby waves. This effect was not considered in *Saenko* (2006).

Modifications to the background stratification and mean flows are observed between pre-industrial and climate-change runs in the GFDL CM4 model (Fig.5.12). However, the question of the quantification of these effects on the Rossby wave activity, as well as the changes induced by a modified background mean flow, is still unanswered. We expect to show considerable alterations to the Rossby wave phase speeds at different latitudes, leading to important changes in the ocean adjustment time-scale and coupled ocean-atmosphere interactions where Rossby waves set the clock (Fig.5.13 and Fig.5.14).

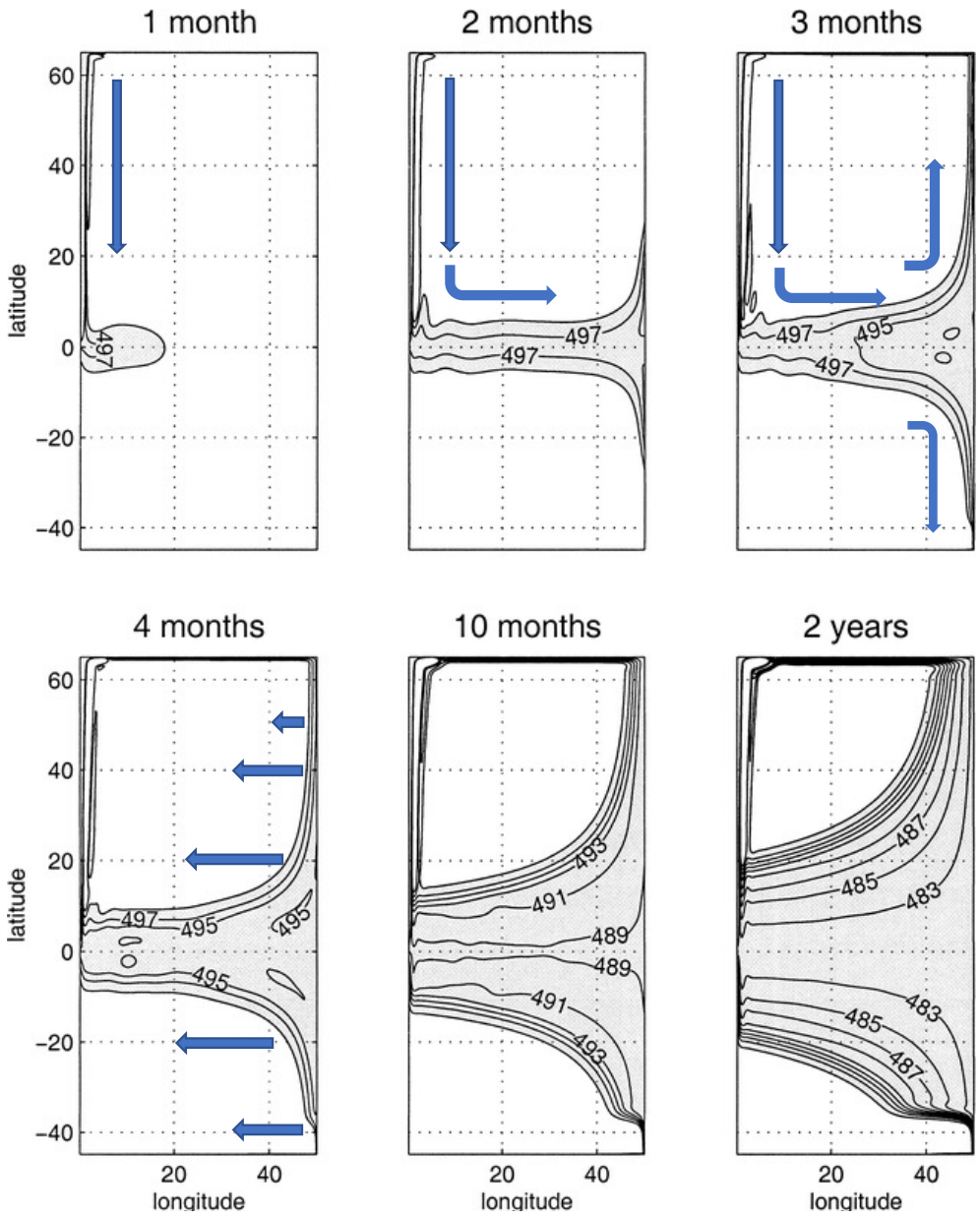

Figure 5.11: *Surface layer thickness after a thermohaline overturning of 10 Sv is switched on at time t = 0 in the northwest corner of an ocean initially at rest. There is no wind forcing, and the surface layer is initially 500 m deep. The contour interval is 2 m, and thicknesses less than 499 m are shaded. Note that the thickness anomaly on the western boundary is much greater than that in the interior. [from Johnson and Marshall, JPO2022]*

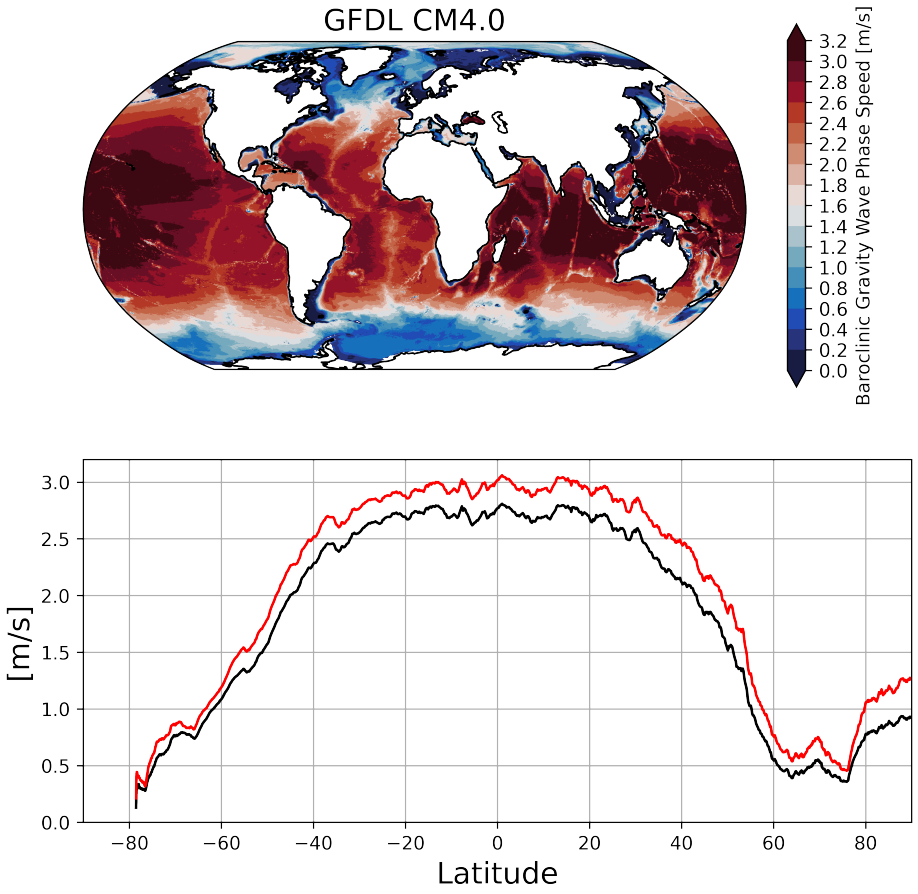

Figure 5.12: *The baroclinic gravity wave phase speed computed from the GFDL-CM4.0 model under historical conditions for years 2010-2014 (in black) and for the future scenario SSP585 (in red).*

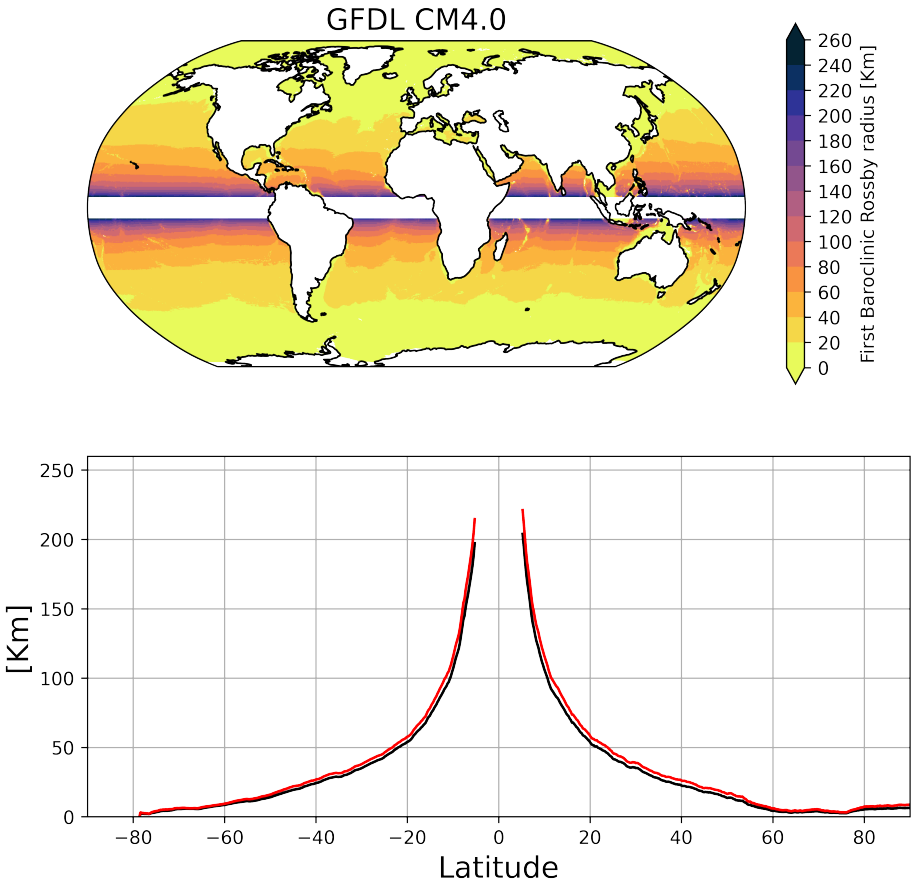

Figure 5.13: *The Rossby radius computed from the GFDL-CM4.0 model under historical conditions for years 2010-2014 (in black) and for the future scenario SSP585 (in red).*

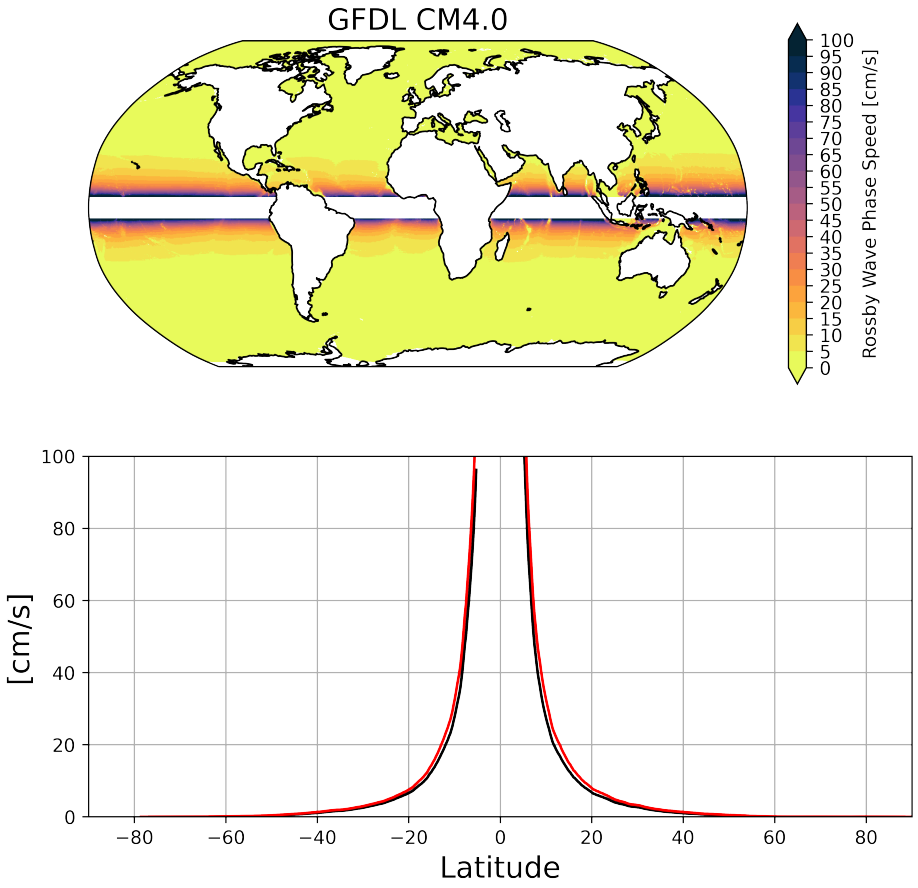

Figure 5.14: *The baroclinic Rossby wave phase speed computed from the GFDL-CM4.0 model under historical conditions for years 2010-2014 (in black) and for the future scenario SSP585 (in red).*

Bibliography

Anderson, D. L. T., and A. E. Gill, Spin-up of a stratified ocean, with application to upwelling, *Deep-Sea Res.*, *22*, 583–596, 1975.

Anderson, D. L. T., and A. E. Gill, Beta-dispersion of inertial waves, *J. Geophys. Res.*, *84*, 1836–1842, 1979.

Cessi, P., and P. Otheguy, Oceanic teleconnections: Remote response to decadal wind forcing, *J. Phys. Oceanogr.*, *33*, 1604–1617, 2003.

Chelton, D. B., and M. G. Schlax, Global observations of oceanic rossby waves, *Science*, ***272***, 234–238, 1996.

Chelton, D. B., R. A. deSzoeke, M. G. Schlax, K. E. Naggar, and N. Siwertz, Geographical variability of the first baroclinic rossby radius of deformation, *J. Phys. Oceanogr.*, ***28***, 433–460, 1998.

Cipollini, P., D. Cromwell, P. G. Challenor, and S. Raffaglio, Rossby waves detected in global ocean colour data, *Geophys. Res. Lett.*, ***28***, 323–326, 2001.

Dewar, W., On ocean dynamics in midlatitude climate, *J. Climate*, ***14***, 4380–4397, 2001.

Dickinson, R. E., Rossby waves-long period oscillations of oceans and atmosphere, *Annu. Rev. Fluid Mech.*, ***10***, 159–195, 1978.

Galanti, E., and E. Tziperman, A midlatitude-enso teleconnection mechanism via baroclinically unstable long rossby waves, *J. Phys. Oceanogr.*, ***33***, 1877–1888, 2003.

Gill, A. E., *Atmosphere-Ocean Dynamics*, *International Geophysics Series*, vol. **30**, 662 pp., Academic Press, 1982.

Hill, K. L., I. Robinson, and P. Cipollini, Propagation characteristics of extratropical planetary waves observed in the atsr global sea surface temperature record, *J. Geophys. Res.*, ***105***, 21,927–21,945, 2000.

Hough, S., On the application of harmonic analysis to the dynamical theory of the tides, part i, on laplace's oscillations of the first species, and on the dynamics of ocean currents, *Phil. Trans. Roy. Soc. Lond.*, *189*, 201–257, 1897.

Hughes, C. W., Rossby waves in the southern ocean: A comparison of topex/poseidon altimetry with model predictions, *J. Geophys. Res.*, ***100***, 15,933–15,950, 1995.

Johnson, H. L., and P. Marshall, A theory for the surface atlantic response to thermohaline variability, *J. Phys. Oceanogr.*, ***32***, 1121–1132, 2002.

Kawase, M., Establishment of deep ocean circulation driven by deep-water production, *J. Phys. Oceanogr.*, ***17***, 2294–2317, 1987.

Killworth, P. D., and J. R. Blundell, The effect of bottom topography on the speed of long extratropical planetary waves, *J. Phys. Oceanogr.*, ***29***, 2689–2710, 1999.

Killworth, P. D., D. B. Chelton, and R. A. de Szoeke, The speed of observed and theoretical long extratropical planetary waves, *J. Phys. Oceanogr.*, ***27***, 1946–1966, 1997.

Leblond, P. H., and L. A. Mysak, *Waves in the Ocean*, 1st ed., 602 pp., Elsevier Oceanography Series, 1981.

Pedlosky, J., *Geophysical Fluid Dynamics*, 2nd ed., Springer-Verlag, 724 pp, 1987.

Pierce, D., T. P. Barnett, N. Schneider, R. Saravanan, D. Dommenget, and M. Latif, The role of ocean dynamics in producing decadal climate variability in the north pacific, *Climate Dyn.*, *18*, 51–70, 2001.

Saenko, O. A., Influence of global warming on baroclinic rossby radius in the ocean: a model intercomparison, *J. Climate*, *19*, 1354–1360, 2006.

Talley, L., Simple coupled midlatitude climate models, *J. Phys. Oceanogr.*, ***29***, 2016–2037, 1999.